Faraday Discussions

Accepted Manuscript

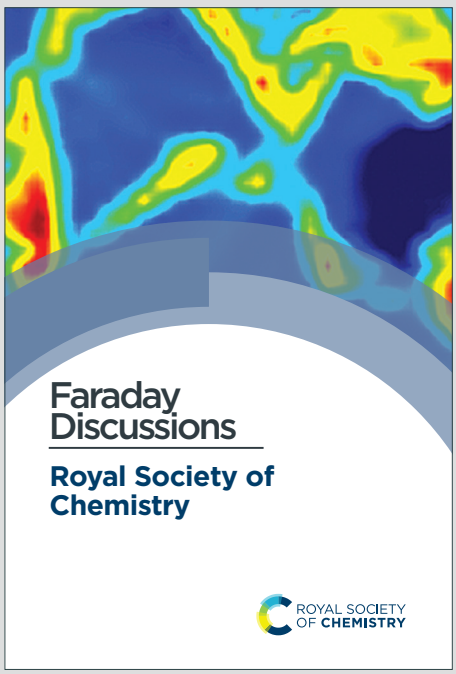

This article can be cited before page numbers have been issued, to do this please use: G. Salinas, S. ARNABOLDI, P. Garrigue, G. Bonetti, R. Cirilli, T. Benincori and A. Kuhn, *Faraday Discuss.*, 2023, DOI: 10.1039/D3FD00041A.

ROYAL SOCIETY OF CHEMISTRY

www.rsc.org/faraday_d

View Article Online
DOI: 10.1039/D3FD00041A

ARTICLE

Magnetic field-enhanced redox chemistry on-the-fly for enantioselective synthesis

Gerardo Salinas,†[a] Serena Arnaboldi,†[b] Patrick Garrigue,[a] Giorgia Bonetti,[c] Roberto Cirilli,[d] Tiziana Benincori[c] and Alexander Kuhn*[a]

Chemistry on-the-fly is an interesting concept, extensively studied in recent years due to its potential use for recognition, quantification and conversion of chemical species in solution. In this context, chemistry on-the-fly for asymmetric synthesis is a promising field of investigation, since it can help to overcome mass transport limitations, present for example in conventional organic electrosynthesis. Herein, the synergy between a magnetic field-enhanced self-electrophoretic propulsion mechanism and enantioselective redox chemistry on-the-fly is proposed as an efficient concept to boost the stereoselective conversion. We employ Janus swimmers as redox-active elements, exhibiting a well-controlled clockwise or anticlockwise motion with a speed that can be increased by one order of magnitude in the presence of an external magnetic field. While moving, these bifunctional objects convert spontaneously on-the-fly a prochiral molecule into a specific enantiomer with high enantiomeric excess. The magnetic field-enhanced self-mixing of the swimmers, based on the formation of local magnetohydrodynamic vortices, leads to an significant improvement of the reaction yield and the conversion rate.

Received 00th January 20xx,
Accepted 00th January 20xx

DOI: 10.1039/x0xx00000x

1. Introduction

Chemistry on-the-fly is a concept defined as the localized chemical conversion of a substance into a desired product *via* a specifically functionalized mobile platform.[1] In recent years, this approach has gained considerable attention in the field of micro and nano swimmers, since the intrinsic high active surface and continuous motion enables a localized mixing of the reactants.[1,2] The efficiency of these self-propelled miniaturized reactors has been extensively exploited for a wide range of physico-chemical systems, ranging from organic pollutant degradation[3-7] to metal ion removal[8-10] and biorecognition.[11-13] In this context, the possible enantiodiscrimination, quantification and synthesis of chiral analytes *via* chemistry-on-the-fly approaches is an interesting challenge. Recently, different enantioselective self-propelled devices have been designed by functionalizing the swimmer surface with different chiral recognition elements, e.g. cyclodextrins, D- or L-amino acid oxidase and also inherently chiral oligomers.[14-16] In particular the latter approach presents outstanding enantioselectivity, related to diastereomeric interactions between the chiral oligomer surface and the analyte antipodes in solution, resulting in thermodynamic differences in terms of redox potentials, which allow the preferential conversion of only one of the analyte enantiomers.[17,18] This energetic differentiation has been exploited to design unconventional approaches for the electrochemical recognition of chiral probes.[19-21] Furthermore, these oligomeric systems were used for the enantioselective conversion of molecules with a prostereogenic carbon-oxygen double bond into the corresponding chiral hydroxyl derivatives *via* chemistry-on-the-fly.[22] In particular, self-propelled Zn particles, functionalized with oligomers of 2,2-bis[2-(5,2-bithienyl)]-3,3-bithianaphthene (BT_2T_4), were employed as mobile microreactors for the enantioselective synthesis of the antipodes of phenyl ethanol and mandelic acid. This approach is based on the coupling of the spontaneous oxidation of Zn in acid media, acting as a source of electrons, and the enantioselective reduction of the prochiral starting compound on the surface of the inherently chiral oligomer. The dynamic behaviour of such Zn/BT_2T_4 hybrid objects induces a continuous mixing of the solution, allowing a more efficient renewal of the prochiral starting compound at the swimmer interface, overcoming the characteristic mass transport limitations of conventional electroorganic synthesis.[23-26] However, the

[a] Univ. Bordeaux, CNRS, Bordeaux INP, ISM UMR 5255 33607 Pessac (France)
[b] Dip. Di Chimica, Univ. degli Studi di Milano 20133 Milan (Italy)
[c] Dip. di Scienza e Alta Tecnologia, Univ. degli Studi dell'Insubria 22100 Como (Italy)
[d] Istituto Superiore di Sanità, Centro Nazionale per il Controllo e la Valutazione dei Farmaci 00161 Rome (Italy)
† These authors contributed equally:
Electronic Supplementary Information (ESI) available: [details of any supplementary information available should be included here]. See DOI: 10.1039/x0xx00000x

View Article Online
DOI: 10.1039/D3FD00041A

motion is triggered by an asymmetric formation/release of bubbles which partially block the active surface area of the device, and thus might decrease the global yield of the stereoselective conversion.

An interesting concept to enhance the mixing of the solution in a more controlled and efficient way, is to induce a local Lorentz force on the ion flux present around the self-electrophoretic device. In general, the presence of a magnetic field, orthogonal to an electrode surface, generates a Lorentz force which triggers the formation of a magnetohydrodynamic (MHD) flow along the edges of the electrode.[27,28] This phenomenon has been extensively explored for improving the overall reaction kinetics e.g. in electrocatalysis and electrodeposition of metals and polymers.[29-31] Furthermore, due to the possibility to control the fluid flow around the electrode surface, this concept has been also extended to redox magnetohydrodynamic microfluidics and self-propulsion of active matter.[31-34] Recently, the synergy between the spontaneous ion flux produced by self-electrophoretic swimmers and an external magnetic field was proposed as an interesting alternative to boost their propulsion speed by up to 2 orders of magnitude.[35] These Lorentz force-driven Janus swimmers exhibit a predictable clockwise or anticlockwise rotational motion as a function of the magnetic field orientation. The concept is complementary to already well-studied magnetic field-driven swimmers, where motion is triggered either by a pulling mechanism or rotating/undulating magnetic fields.[36-44] In a first order approximation, the above mentioned Zn/BT_2T_4 swimmers behave as self-electrophoretic systems, with a flux of cations from the anodic to the cathodic sites of the Janus object (or *vice versa* for anions), induced by the spontaneous redox reactions. Thus, we propose in the present contribution the use of this ion flux, in combination with an external magnetic field, to design swimmers able to perform redox chemistry on-the-fly for enantioselective synthesis. The synergy between these two main ingredients provides a substantial boost of the dynamic behaviour of the redox swimmers, reflected by an improved efficiency of the stereoselective conversion.

2. Experimental

2.1. Electrosynthesis of enantiopure oligo-(*R*)-BT_2T_4 or oligo-(*S*)-BT_2T_4.

Zn wires, modified with a thin Pt layer were obtained by spontaneous deposition of Pt when dipping a zinc wire (GoodFellow, 99.99%, d = 250 µm) in a 20 mM H_2PtCl_6 solution under constant stirring for 2 minutes. Electrogeneration of the enantiopure oligo-(*R*)-BT_2T_4 or oligo-(*S*)-BT_2T_4 (Figure 1a) was carried out on these core/shell wires in a vial containing 5 cm^3 of a 0.1 M solution of lithium perchlorate ($LiClO_4$; Sigma-Aldrich) in acetonitrile (MeCN; Sigma-Aldrich) and 5 mM of the (*R*)- or (*S*)-enantiopure monomers. The three-electrode system was composed of the Zn/Pt wire, a Pt wire and a Ag wire, acting as working, counter and pseudo-reference electrodes, respectively. The potentiodynamic synthesis of the oligomers was performed by applying a potential sweep from 0 V to 1.2 V, with a constant scan rate (100 mV s^{-1}) for 36 cycles. All electrochemical experiments were carried out with a PalmSense potentiostat connected to a personal computer.

2.2. Characterization.

The morphology and composition of the Zn/Pt/oligo-(*R*)-BT_2T_4 or (*S*)-BT_2T_4 hybrid device was characterized by scanning electron microscopy and energy-dispersive X-ray spectroscopy, using a Vega3 Tescan 20.0 kV microscope.

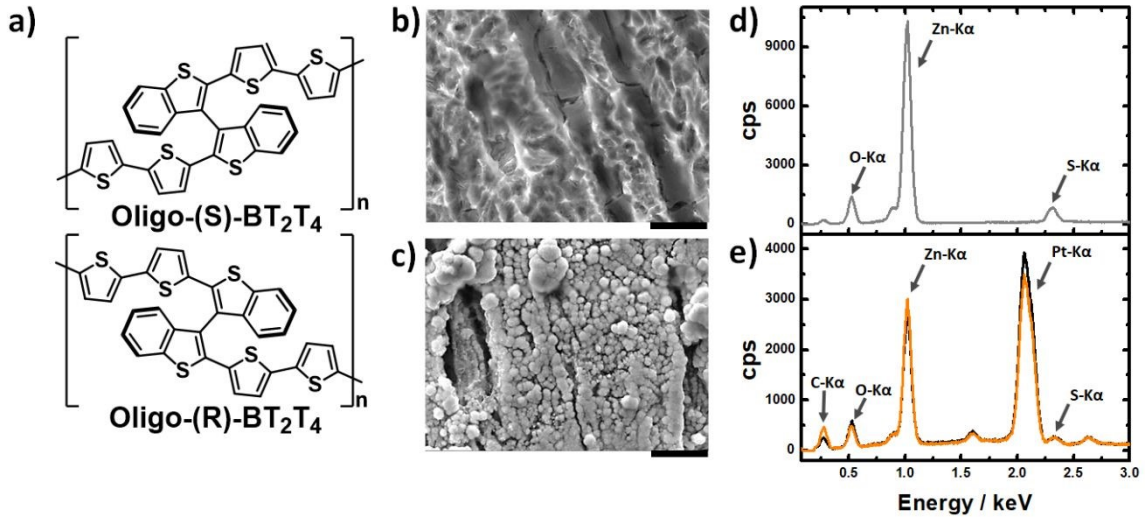

Fig. 1 a) Chemical structures of the oligo-(*S*) and oligo-(*R*)-2,2-bis[2-(5,2-bithienyl)]-3,3-bithianaphthene (oligo(*S*)- and oligo-(*R*)-BT_2T_4). SEM images of the surface of b) a pristine and c) Pt/oligo-BT_2T_4 modified Zn surface. Scale bar 5 µm. EDX signals around the emission peaks of carbon, oxygen, zinc, platinum and sulphur of d) a pristine Zn wire and e) a Zn/Pt (black line) and a Zn/Pt/oligo-BT_2T_4 (orange line) hybrid device.

2.3. Enantioselective synthesis with the redox chemistry-on-the-fly swimmers.

After depositing the respective oligo-BT_2T_4 enantiomers, the hybrid wire was cut into short pieces, leading to swimmers where at both cross sections bare Zn is exposed (average length of 1.1 mm ± 0.2 mm; diameter of 250 µm). In order to break the symmetry of the devices, one Zn face was carefully covered with varnish (Scheme S1). For the enantioselective synthesis, six of these Janus swimmers were positioned at the air/water interface of a 0.1 M H_2SO_4 aqueous solution containing 50 mM of acetophenone (AP) for 1 hour. For the redox synthesis in the presence of a magnetic field, a rectangular FeNdB magnet (B = 200 mT, Area = 98 cm^2) was placed below the reaction chamber. After one hour, the products were extracted with heptane and the solution was analyzed on a Jasco HPLC machine (LC-4000) equipped with a photodiode array (PDA) and CD detectors at a wavelength of 210 nm and 260 nm, respectively. HPLC analysis was carried out by using a chiral column Chiralpak IB N-5 (250 × 4.6 mm, 5 µm) and a n-heptane/2-propanol 92:8 (v/v) mixture as mobile phase (flow rate = 0.5 mL min^{-1}). The dynamic behaviour of the swimmers was monitored by using a CCD camera (CANON EOS 70D, Objective Canon Macro Lens 100 mm 1:2.8). Video processing and tracking was performed with ImageJ software.

3. Results and discussions

The hybrid swimmers were designed by following a two-step approach. First, the macroscopic Zn wire was modified with a thin Pt shell (7 µm ± 1 µm) by the spontaneous reduction of $PtCl_6^{2-}$, to guarantee a good electrical contact between the Zn core and the corresponding oligomer. In the second step, the inherently chiral oligomer was generated by the potentiodynamic oligomerization of (*R*)-BT_2T_4 and (*S*)-BT_2T_4, respectively (Figure 1a). In order to study the composition and evaluate the changes in morphology, scanning electron microscopy (SEM) analysis (Figure 1b and c), coupled with energy dispersive X-ray spectrometry (EDS) (Figure 1d and e), was carried out with a 1 cm long Zn/Pt/oligo-BT_2T_4 wire. Three different regions have been examined, the pristine Zn wire, a Zn/Pt region and a hybrid Zn/Pt/oligo-BT_2T_4 section. As can be seen from the SEM images, the hybrid region presents a porous globular morphology in comparison to pristine Zn (Figure 1b and c). The EDX signal for the bare Zn extremity shows the presence of mainly zinc (Zn-Kα), oxygen (O-Kα) and sulphur (S-Kα), probably due to the formation of zinc sulphate during the cleaning of the wire (Figure 1d). The Zn/Pt part of the wire presents characteristic signals of platinum (Pt-Kα) (Figure 1e, black line), which decrease for the hybrid part of the device, accompanied by an increase of the carbon signal (C-Kα) (Figure 1e, orange line), evidencing the presence of the conjugated oligomer on top of the platinum surface.

After this first characterization of the composition of the Zn/Pt/oligo-BT_2T_4 objects, the propulsion mechanism, driven by the induced Lorentz-force, was examined. Since the use of inherently chiral molecules allows the control of the stereochemical outcome of a reaction, these hybrid materials are an interesting ingredient for asymmetric organic conversions. In this context, we have chosen as a model reaction, the reduction of the ketone moiety of a prochiral precursor, acetophenone, leading to the corresponding enantiomers of 1-phenylethanol (1-PE). Theoretically, in an acidic solution, the oxidation of Zn and the reduction of protons on Pt occur spontaneously with a standard redox potential difference of 0.76 V. Under these conditions, and in the

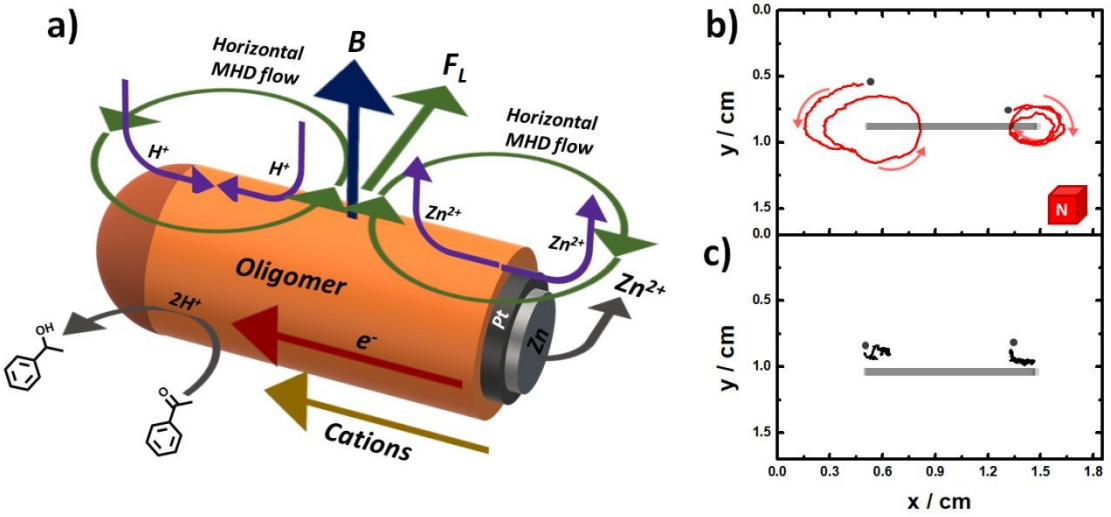

Fig. 2 a) Schematic illustration of the formation of the MHD-flow on the surface of a self-propelled swimmer with a representation of the associated chemical reactions, the spontaneous ionic currents, the magnetic field B, the induced Lorentz force F_L and the resulting MHD convection. b) Tracking of the trajectory of a tracer particle (glassy carbon bead, Ø = 500 – 1000 µm) moving on the air/water interface (0.1 M H_2SO_4 and 50 mM AP) above a macroscopic Zn/Pt/oligo-BT_2T_4 device in the presence of a magnetic field (north pole up). c) Same experiment as in (b), but in the absence of the magnetic field. The grey dots indicate the initial position of the tracer particle.

View Article Online
DOI: 10.1039/D3FD00041A

presence of the inherently chiral surface, a certain fraction of the produced electrons can be used to trigger the asymmetric reduction of the prochiral molecule to only one of the enantiomers (Figure 2a). The intrinsic electron flux from the anodic to the cathodic part of the device is accompanied by a movement of ions towards or away from the outer surface at each extremity of the Janus object (Figure 2a, pink arrows). As stated above, in the presence of a magnetic field, orthogonal to the air/water interface, the resulting Lorentz force induces the formation of a MHD flow at each extremity of the device (Figure 2a, green circles). In order to visualize both MHD vortices in the vicinity of the swimmer, a macro-Zn/Pt/oligo-BT_2T_4 object (l ≈ 1 cm), was immobilized below the air/water interface of a 100 mM H_2SO_4, 50 mM AP solution. The set-up was placed at the center of a rectangular FeNdB magnet (B ≈ 200 mT, A = 98 cm^2) with the north pole facing upwards. A glassy carbon bead (Ø = 500 – 1000 µm), acting as a tracer particle, was positioned at the air/water interface in two different regions of the device. Two circular hydrodynamic flow patterns, with a specular clockwise and anticlockwise orientation, are formed above the wire (Figure 2b and Video S1). The circular motion exhibits an oscillating speed, which can be correlated with the relative position of the bead moving above the hybrid wire (Figure S1). Maximum speed values of 0.8 mm/s and 1.5 mm/s (above the Zn cross section and the Pt/oligo-BT_2T_4 region, respectively), are recorded when the tracer bead is closest to the middle part of the device. The difference in size of the circular hydrodynamic flow patterns and the maximum speed values, depend on the size of the active surface where each reaction is taking place. Thus, since the oxidation of Zn occurs only at the cross section of the wire where the bare metal is exposed, a rather focused MHD vortex is produced. On the contrary, as the reduction of prochiral molecules and consumption of protons takes place everywhere along the Pt/oligo-BT_2T_4 surface, this causes the formation of stronger MHD flow with a larger vortex diameter. This continuous mixing of the solution, induced by the two cooperating MHD vortices, should increase the mass transport of the prochiral compound towards the catalytic surface, thus improving the overall production rate. In strong contrast to these experiments, only random motion of the tracer particle is observed in the absence of the magnetic field (Figure 2c and Video S1).

After this characterization of the MHD flow at the macroscopic scale, the influence of the orientation of the magnetic field on the displacement of miniaturized Janus swimmers has been studied during the redox conversion of AP to 1-PE. Six Janus Zn/Pt/oligo-(R)-BT_2T_4 swimmers, with an average length of 1.1 mm ± 0.2 mm, were positioned at the air/water interface of a 100 mM H_2SO_4, 50 mM AP solution, allowing them to move freely for 1 hour. The set-up was placed at the center of a rectangular FeNdB magnet (B ≈ 200 mT, A = 98 cm^2) with either the north or south pole facing upwards. The MHD vortices, observed at the macroscopic scale (*vide supra*), should provide also at these smaller scales a significant driving force to continuously propel the swimmers.

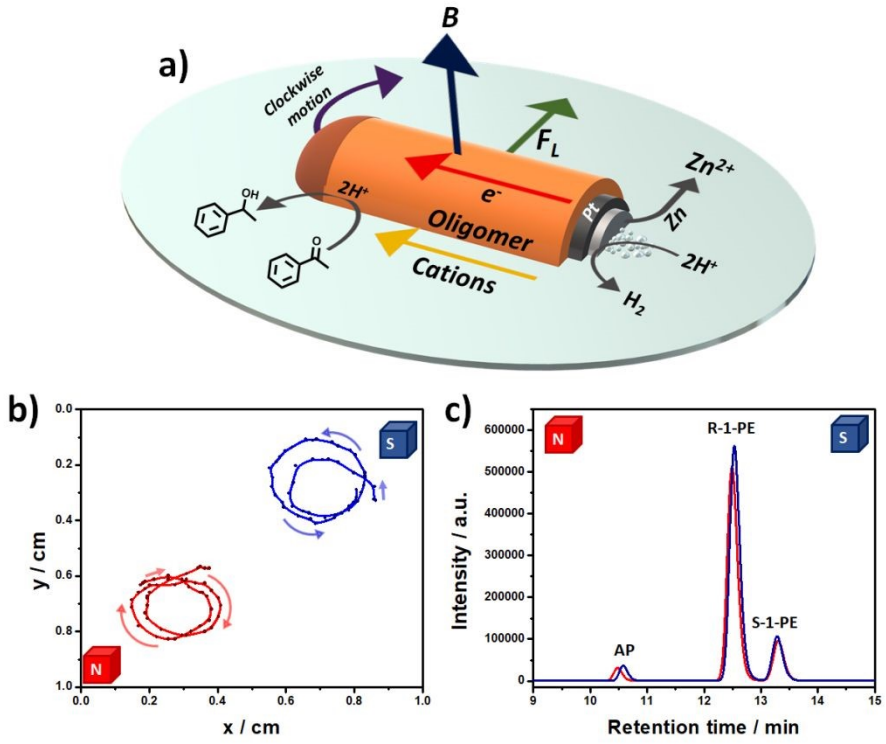

Fig. 3 a) Schematic illustration of the clockwise motion of a self-propelled Janus swimmer with a representation of the associated chemical reactions, the spontaneous ionic currents, the magnetic field B and the resulting Lorentz force F_L. b) Tracking plots of two individual Zn/Pt/oligo-(*R*)-BT_2T_4 swimmers moving at the air/water interface of a 0.1 M H_2SO_4 and 50 mM AP solution, as a function of the magnetic field orientation (indicated in the figure). c) Chromatograms of the product mixtures obtained after 1 hour of asymmetric synthesis carried out by the continuous displacement of 6 Zn/Pt/oligo-(*R*)-BT_2T_4 swimmers placed at the air/water interface of a 0.1 M H_2SO_4 and 50 mM AP solution, as a function of the magnetic field orientation (indicated in the figure).

View Article Online
DOI: 10.1039/D3FD00041A

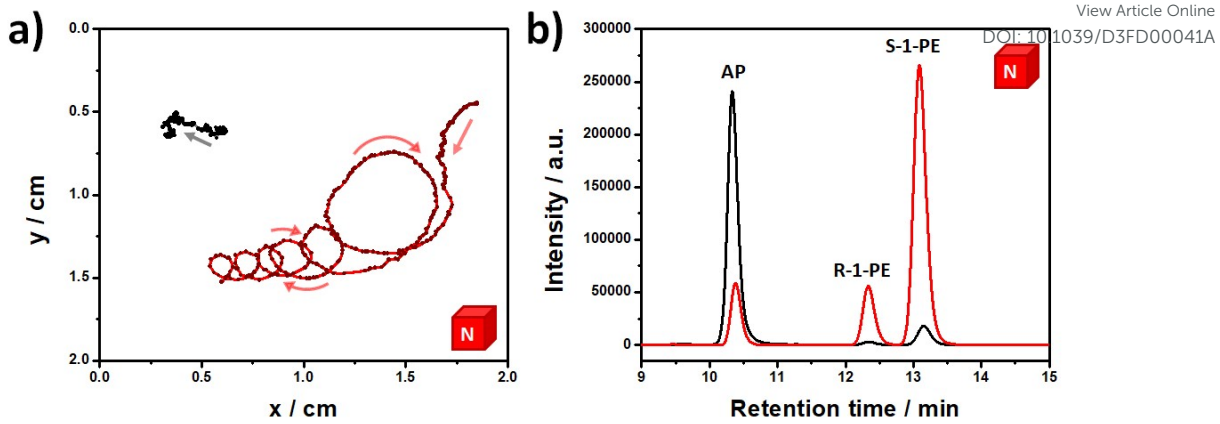

Fig. 4 a) Tracking plots of two individual Zn/Pt/oligo-(*S*)-BT_2T_4 swimmers moving at the air/water interface of a 0.1 M H_2SO_4 and 50 mM AP solution, in the absence (black line) and in the presence (red line) of an orthogonal magnetic field (north pole upwards). b) Chromatograms of the product mixtures obtained after 1 hour of asymmetric synthesis carried out by 6 Zn/Pt/oligo-(*S*)-BT_2T_4 swimmers, placed at the air/water interface of a 0.1 M H_2SO_4 and 50 mM AP solution, in the absence (black line) and in the presence (red line) of an orthogonal magnetic field (north pole upward).

However, as these objects are no longer immobilized, like in the previous experiments, an additional Lorentz force, which acts on the ion flux parallel to the main axis of the object, has to be taken into account (Figure 3a, yellow arrow).[35] This contributes to the overall displacement of the swimmer, by causing a torque force that translates into a predictable clockwise or anticlockwise motion, as a function of the orientation of the magnetic field.

Consequently, the Janus swimmers present a clockwise motion when the north pole of the magnet is orientated upwards, whereas an anticlockwise rotation is observed by inverting the orientation of the magnetic field (south pole upwards) (Figure 3b, Video S2 for single swimmers and Video S3 for an ensemble of swimmers). After one hour of self-mixing, the products of the stereoselective reaction were extracted with heptane and analyzed by enantioselective HPLC. As mentioned previously, the spontaneous oxidation of Zn is the driving force of the enantioselective reduction of the prochiral compound, since a fraction of the liberated electrons is shuttled to the inherently chiral surface. Thus, by functionalizing the surface of the swimmers with only one enantiomer of oligo-BT_2T_4, in this case the (*R*)-oligomer, the enantioselective reduction of AP to R-1-PE is expected. From the analysis of the HPLC chromatograms it was possible to confirm the transformation of AP into R-1-PE with a yield of ≈ 80% ± 4% and an %ee of ≈ 70% ± 1%, independent of the magnetic field orientation (Figure 3c, red curve for north pole up and blue curve for south pole up, respectively). The high stereoselectivity was confirmed by chromatograms with online circular dichroism detection, where the negative and positive signals can be associated to the synthesis of the (*R*)- and (*S*)-enantiomer, respectively (Figure S2). Again, the enantioselectivity does not depend on the orientation of the magnetic field, showing that the stereoselective reaction is not influenced by any spin polarization effect.[45-47]

Using the same experimental conditions, we have evaluated the magnetic field enhancement of the redox conversion by comparing the yield of the reaction in the absence and in the presence of an orthogonal magnetic field. Six Janus Zn/Pt/oligo-(*S*)-BT_2T_4 swimmers, (l = 1.1 mm ± 0.2 mm), were positioned at the air/water interface of a 100 mM H_2SO_4, 50 mM AP solution, allowing them to move freely for 1 hour. The set-up was placed at the center of a rectangular FeNdB magnet (B ≈ 200 mT, A = 98 cm^2) with the north pole facing upwards. Under exactly the same conditions, an independent experiment was carried out with six freshly modified oligo-(*S*)-BT_2T_4 swimmers without magnet. In the presence of the magnetic field, the self-propelled devices present a clockwise motion with an average speed of 0.7 mm/s ± 0.1 mm/s, which is roughly one order of magnitude faster than the one measured for the random motion in the absence of the magnet (0.1 mm/s ± 0.03 mm/s) (Figure 4a and Video S4). The stereoselectivity of the reaction is preserved, since both redox conversions present a similar %ee value (≈70%), however the enantioselective synthesis in the presence of the magnetic field leads to higher yields (≈80%) in comparison with the low value measured for the experiment without magnet (≈10 %), as illustrated in Figure 4b. This is due to the self-mixing capabilities of the swimmers, based on the magnetic field induced motion.

In a control experiment, the dynamic behaviour and the yield of products generated by the spontaneous motion of six achiral Janus Zn/Pt swimmers, were tested. For comparison, these objects were positioned at the air/water interface of a 100 mM H_2SO_4, 50 mM AP solution, with the north pole facing upwards for 1 hr. The Janus swimmers present a clockwise motion with an average speed of 0.4 mm/s ± 0.1 mm/s and a very low conversion (≈0.5%) (Figure S3 and Video S5). These results indicate that in this case, the large majority of the electrons liberated by the dissolution of zinc is used for the reduction of protons, as this reaction is

View Article Online
DOI: 10.1039/D3FD00041A

thermodynamically and kinetically favoured on platinum, compared to the reduction of the prochiral molecule. There is also a significant difference in speed, in comparison with the swimmers modified with the inherently chiral oligomer, since the continuous production of H_2 bubbles everywhere on the Pt shell does not allow an as efficient directional propulsion of the Zn/Pt objects. As expected, in the case of achiral swimmers, the %ee is zero within error bars. Finally, in order to compare the conversion efficiency, the reaction rate of AP was calculated for achiral and chiral swimmers (see supporting information for details). In the presence of the orthogonal magnetic field, values of 0.001 mmol h^{-1} mm^{-1} and 0.30 mmol h^{-1} mm^{-1} were obtained for the Zn/Pt and the Zn/Pt/oligo-(*S*)-BT_2T_4 swimmers, respectively. Once again, this provides evidence that the presence of the inherently chiral oligomer not only induces stereoselectivity, but also greatly promotes the global reactivity by more than two orders of magnitude. Furthermore, the efficiency of the redox chemistry-on-the fly is enhanced in the presence of the magnetic field by up to one order of magnitude, in comparison with the conversion in the absence of the magnet (0.03 mmol h^{-1} mm^{-1}), due to an improved mixing of the solution caused by the MHD effect.

Conclusions

We have demonstrated the possibility to boost the propulsion of Zn/Pt/oligo-BT_2T_4 hybrid swimmers, using the effect of magnetohydrodynamic convection (MHD effect). The chiral Janus objects are functionalized with the enantiomers of an inherently chiral oligomer. When they are placed in acidic solutions containing a prochiral starting compound, the spontaneous redox reactions that occur on their surfaces trigger the stereospecific conversion of the prochiral molecule into the desired enantiomer. The inherently helical molecular structure of the polymer provides a chiral environment which is the basis for quite important thermodynamic differences when comparing its interactions with the two antipodes of a given chiral molecule. This naturally also affects the outcome of the reduction of a prochiral ketone into a chiral alcohol if it occurs in such a chiral environment. In the transition state the intermediate species is more likely to evolve towards a final enantiomer with the energetically more favorable stereochemistry, as we have already demonstrated in one of our previous studies.[22]

The magnetic field enhancement of the redox conversion has been evaluated by comparing the yield of an asymmetric model reaction, the reduction of acetophenone into the enantiomers of phenylethanol, in the absence and in the presence of an orthogonal magnetic field. In the presence of a magnet, the Janus swimmers exhibit well-defined clockwise or anticlockwise motion, with an up to one order of magnitude higher speed. This leads to a significant improvement of the reaction yield and of the conversion rate. Without magnet, the reaction is still stereospecific, but proceeds with a one order of magnitude lower conversion rate.

We can conclude that this better performance is based on the fact that the MHD effect, generated by the presence of a magnet, induces controlled active micro-mixing with a more efficient renewal of the prochiral starting compound at the oligomer surface. In addition, the MHD effect facilitates the detachment of bubbles from the swimmer surface, thus partially liberating active surface area, which otherwise would be blocked by the presence of gas. This leads to a considerable increase in the global yield of the stereoselective conversion. Moreover, in contrast to other concepts of magnetically driven macro-, micro- and nano swimmers described in the literature, where the presence of a ferromagnetic component is mandatory to trigger motion,[48] the here presented approach allows to take advantage, in an unconventional way, of the synergy between the local electric and global magnetic field, without the need for ferromagnetic constituents in the swimmer architecture. This offers a higher degree of freedom in the design of motile functional devices, for which the presence of an external magnet will lead to a more efficient propulsion. With respect to future applications, these chiral Janus swimmers might be potentially used for the scale-up of asymmetric reduction processes. Furthermore, the magnetic field enhanced conversion efficiency could be also of interest for other chemistry-on-the fly applications, as long as redox processes are involved in the reaction mechanism.

Author Contributions

AK: Conceptualization, Funding acquisition, Project administration, Writing – review & editing; GS and SA: Investigation, Data Curation, Writing – review & editing; PG, RC, GB: Investigation; TB: Investigation, Writing – review & editing

Conflicts of interest

There are no conflicts to declare.

Acknowledgements

This work has been funded by the European Research Council (ERC) under the European Union's Horizon 2020 research and innovation program (grant agreement no 741251, ERC Advanced grant ELECTRA) and under the HORIZON-ERC-2021 work program (grant agreement no 101040798, ERC Starting grant CHEIR).

View Article Online
DOI: 10.1039/D3FD00041A

References

1 E. Karshalev, B. Esteban-Fernandez de Avila, J. Wang, *J. Am. Chem. Soc*., 2018, **140**, 3810-3820.
2 Y. Hu, W. Liu, Y. Sun, *Adv. Funct. Mater*., 2022, **32**, 2109181.
3 C. Zheng, X. Song, Q. Gan, J. Lin, *J. Colloid Interface Sci.*, 2023, **630**, 121.
4 M. Bayraktaroglu, B. Jurado-anchez, M. Uygun, *J. Hazard. Mater*., 2021, **418**, 126268.
5 Y. Hu, W. Liu, Y. Sun, *ACS Appl. Mater. Interfaces*, 2020, **12**, 41495-41505.
6 M. Ren, W. Guo, H. Guo, X. Ren, *ACS Appl. Mater. Interfaces,* 2019, **11**, 22761-22767.
7 C. C. Mayorga-Martinez, J. Vyskocil, F. Novotny, M. Pumera, *J. Mater. Chem. A*, 2021, **9**, 14904-14910.
8 D. A. Uygun, B. Jurado-Sanchez, M. Uygun, J. Wang, *Environ. Sci.: Nano*, 2016,**3**, 559-566.
9 W. Yang, J. Li, Y. Lyu, X. Yan, P. Yang, M. Zuo, *J. Clean. Prod*., 2021, **309**, 127294.
10 T. Hou, S. Yu, M. Zhou, M. Wu, J. Liu, X. Zheng, J. Li, J. Wang, X. Wang, *Nanoscale*, 2020,**12**, 5227-5232
11 K. Yuan, C. Cuntin-Abal, B. Jurado-Sanchez, A. Escarpa, *Anal. Chem*., 2021, **93**, 16385-16392.
12 R. Maria-Hormigos, A. Molinero-Fernandez, M. A. Lopez, B. Jurado-Sanchez, A. Escarpa, *Anal. Chem*., 2022, **94**, 5575-5582.
13 A. Molinero-Fernandez, M. Moreno-Guzman, L. Arruza, M. A. Lopez, A. Escarpa, *ACS Sens*., 2020, **5**, 1336-1344.
14 J. Muñoz, M. Urso, M. Pumera, *Angew. Chem. Int. Ed.,* 2022, **134**, e202116090.
15 L. Garcia-Carmona, M. Moreno-Guzman, M. C. Gonzalez, A. Escarpa, *Biosens. Bioelectron*., 2017, **96**, 275-280.
16 S. Arnaboldi, G. Salinas, A. Karajic, P. Garrigue, T. Benincori, G. Bonetti, R. Cirilli, S. Bichon, S. Gounel, N. Mano, A. Kuhn, *Nat. Chem*., 2021, **13**, 1241-1247.
17 S. Arnaboldi, T. Benincori, R. Cirilli, W. Kutner, M. Magni, P. R. Mussini, Noworyta, F. Sannicolo, *Chem. Sci*. 2015, **6**, 1706-1711.
18 G. Salinas, M. Niamlaem, A. Kuhn, S. Arnaboldi, *Curr. Opin. Colloid Interface Sci.*, 2022, **61**, 101626.
19 S. Arnaboldi, G. Salinas, G. Bonetti, R. Cirilli, T. Benincori, A. Kuhn, *ACS Meas. Au* 2021, **1**, 110-116.
20 G. Salinas, S. Arnaboldi, G. Bonetti, R. Cirilli, T. Benincori, A. Kuhn, *Chirality*, 2021, **33**, 875-882.
21 S. Arnaboldi, G. Salinas, G. Bonetti, R. Cirilli, T. Benincori, A. Kuhn, *Biosens. Bioelectron.,* 2022, **218**, 114740.
22 S. Arnaboldi, G. Salinas, G. Bonetti, P. Garrigue, R. Cirilli, T. Benincori, A. Kuhn, *Angew. Chem. Int. Ed.,* 2022, **61**, e202209098.
23 S. B. Beil, D. Pollok, S. R. Waldvogel, *Angew. Chem. Int. Ed.,* 2021, **60**, 14750-14759.
24 S. Mohle, M. Zirbes, E. Rodrigo, T. Gieshoff, A. Wibe, S. R. Waldvogel, *Angew. Chem. Int. Ed*., 2018, **57**, 6018-6041.
25 R. D. Little, *J. Org. Chem*. 2020, **85**, 13375-13390.
26 G. Hilt, *ChemElectroChem* 2020, **7**, 395-405.
27 V. Gatard, J. Deseure, M. Chatenet, *Curr. Opin. Electrochem.,* 2020, **23**, 96-105.
28 Songzhu Luo, K. Elouarzaki, Z. J. Xu, *Angew. Chem. Int. Ed*., 2022, **61**, e202203564
29 Y. Zhang, Ce, Liang, J. Wu, Han, Liu, B. Zhang, Z. Jiang, S. Li, P. Xu, *ACS Appl. Energy Mater*., 2020, **3**, 10303-10316
30 I. Mogi, R. Morimoto, R. Aogaki, *Curr. Opin. Electrochem.*, 2017, **7**, 1-6.
31 G. Salinas, C. Lozon, A. Kuhn, *Curr. Opin. Electrochem.*, 2023, **38**, 101220.
32 F. Z. Khan, J. A. Hutcheson, C. J. Hunter, A. J. Powless, D. Benson, I. Fritsch, T. J. Muldoon, *Anal. Chem*., 2018, **90**, 7862-7870.
33 J. C. Sikes, K. Wonner, A. Nicholson, P. Cignoni, I. Fritsch, K. Tschulik, *ACS Phys. Chem. Au* 2022, **2**, 289-298.
34 A. Zharov, V. Fierro, A. Celzard, *Appl. Phys. Lett*., 2020, **117**, 104101.
35 G. Salinas, K. Tieriekhov, P. Garrigue, N. Sojic, L. Bouffier, A. Kuhn, *J. Am. Chem. Soc*., 2021, **143**, 12708-12714
36 V. M. Kadiri, C. Bussi, A. W. Holle, K. Son, H. Kwon, G. Schütz, M. G. Gutierrez, P. Fischer, *Adv. Mater*., 2020, **32**, 2001114.
37 X. Z. Chen, J. H. Liu, M. Dong, L. Müller, G. Chatzipirpiridis, C. Hu, A. Terzopoulou, H. Torlakcik, X. Wang, F. Mushtaq, J. Puigmarti-Luis, Q. D. Shen, B. J. Nelson, S. Pane, *Mater. Horiz*., 2019, **6**, 1512-1516.
38 S. Sanchez, A. A. Solovev, S. M. Harazim, O. G. Schmidt, *J. Am. Chem. Soc*., 2011, **133**, 701-703
39 T. Qui, T. C. Lee, A. G. Mark, K. I. Morozov, R. Münster, O. Mierka, S. Turek, A. M. Leshansky, P. Fischer, *Nat. Commun*., 2014, **5**, 5119.
40 L. Baraban, D. Makarov, R. Streubel, I. Mönch, D. Grimm, S. Sanchez, O. G. Schmidt, *ACS Nano* 2012, **6**, 3383-3389.
41 A. Ghosh, P. Fischer, *Nano Lett*. 2009, **9**, 2243-2245
42 R. Dreyfus, J. Baudry, M. L. Roper, M. Fermigier, H. A. Stone, J. Bibette, *Nature* 2005, **437**, 862-865.
43 K. E. Peyer, L. Zhang, B. J. Nelson, *Nanoscale* 2013, **5**, 1259-1272.
44 L. Zhang, J. J. Abbott, L. Dong, B. E. Kratochvil, D. Bell, B. J. Nelson, *Appl. Phys. Lett*. 2009, **94**, 064107.
45 R. Naaman, D. H. Waldeck, *J. Phys. Chem. Lett*., 2012, **3**, 2178-2187.
46 R. Naaman, Y. Paltiel, D. H. Waldeck, *Annu. Rev. Biophys*., 2022, **51**, 99-114.
47 Y. Wolf, Y. Liu, J. Xiao, N. Park, B. Yan, *ACS Nano* 2022, **16**, 18601-18607.
48 H. Zhou, C. C. Mayorga-Martinez, S. Pane, L. Zhang, M. Pumera, *Chem. Rev*., 2021, **121**, 8, 4999-5041.